

# THE ORIGIN OF THE PROMPT EMISSION FOR SHORT GRB 170817A: PHOTOSPHERE EMISSION OR SYNCHROTRON EMISSION?

YAN-ZHI MENG<sup>1,2</sup>, JIN-JUN GENG<sup>3,4</sup>, BIN-BIN ZHANG<sup>3,4</sup>, JUN-JIE WEI<sup>1</sup>, DI XIAO<sup>3,4</sup>, LIANG-DUAN LIU<sup>3,4</sup>, HE GAO<sup>5</sup>,  
 XUE-FENG WU<sup>1</sup>, EN-WEI LIANG<sup>6</sup>, YONG-FENG HUANG<sup>3,4</sup>, ZI-GAO DAI<sup>3,4</sup>, BING ZHANG<sup>7</sup>

<sup>1</sup>Purple Mountain Observatory, Chinese Academy of Sciences, Nanjing 210008, China; xfwu@pmo.ac.cn

<sup>2</sup>University of Chinese Academy of Sciences, Beijing 100049, China

<sup>3</sup>School of Astronomy and Space Science, Nanjing University, Nanjing 210093, China; gengjinjun@nju.edu.cn, zhang.grb@gmail.com

<sup>4</sup>Key Laboratory of Modern Astronomy and Astrophysics (Nanjing University), Ministry of Education, China

<sup>5</sup>Department of Astronomy, Beijing Normal University, Beijing 100875, China

<sup>6</sup>Department of Physics and GXU-NAOC Center for Astrophysics and Space Sciences, Guangxi University, Nanning 530004, China and

<sup>7</sup>Department of Physics and Astronomy, University of Nevada, Las Vegas, NV 89154, USA

*Draft version August 27, 2018*

## ABSTRACT

The first gravitational-wave event from the merger of a binary neutron star system (GW170817) was detected recently. The associated short gamma-ray burst (GRB 170817A) has a low isotropic luminosity ( $\sim 10^{47}$  erg s<sup>-1</sup>) and a peak energy  $E_p \sim 145$  keV during the initial main emission between -0.3 and 0.4 s. The origin of this short GRB is still under debate, but a plausible interpretation is that it is due to the off-axis emission from a structured jet. We consider two possibilities. First, since the best-fit spectral model for the main pulse of GRB 170817A is a cutoff power law with a hard low-energy photon index ( $\alpha = -0.62^{+0.49}_{-0.54}$ ), we consider an off-axis photosphere model. We develop a theory of photosphere emission in a structured jet and find that such a model can reproduce a low-energy photon index that is softer than a blackbody through enhancing high-latitude emission. The model can naturally account for the observed spectrum. The best-fit Lorentz factor along the line of sight is  $\sim 20$ , which demands that there is a significant delay between the merger and jet launching. Alternatively, we consider that the emission is produced via synchrotron radiation in an optically thin region in an expanding jet with decreasing magnetic fields. This model does not require a delay of jet launching but demands a larger bulk Lorentz factor along the line of sight. We perform Markov Chain Monte Carlo fitting to the data within the framework of both models and obtain good fitting results in both cases.

*Subject headings:* gamma-ray burst: general — radiation mechanisms: thermal — gravitational waves

## 1. INTRODUCTION

Recently, the first joint detection of gravitational wave (GW) event (GW170817; Abbott et al. 2017a) and short gamma-ray burst (GRB 170817A; Abbott et al. 2017b; Connaughton et al. 2017; Goldstein et al. 2017a; Savchenko et al. 2017) confirmed the hypothesis that mergers of the double neutron stars (NS–NS) are the progenitor systems of short gamma-ray bursts (SGRBs; Eichler et al. 1989; Narayan et al. 1992; Mochkovitch et al. 1993; Nakar 2007; Berger 2014). Follow-up electromagnetic observations revealed a host galaxy of GRB 170817A at a distance of  $\sim 40$  Mpc (Coulter et al. 2017), as well as broad-band emission (Abbott et al. 2017c). The isotropic-equivalent energy of GRB 170817A is  $\sim 5 \times 10^{46}$  erg (Goldstein et al. 2017; Zhang et al. 2018b), which is much smaller than that of a typical SGRB ( $10^{50}$  erg).

Previous observations of short GRB jet breaks suggested that the half opening angle of a SGRB jet is  $\leq 20^\circ$  (e.g. Fong et al. 2015). On the other hand, the GW signals are essentially isotropic, so the detection rate of a GW event associated with an on-axis burst should be quite low for binary NS mergers. However, the simultaneous detection of GRB 170817A and GW170817 indicates that the rate for such similar events is actually high (Zhang et al. 2018b). Such a high rate im-

plies that the jet may be structured, with an angle-dependent luminosity and bulk Lorentz factor outside an uniform core, rather than a simple ‘top-hat’ form with a sharp edge (Granot et al. 2017a). Emission from such a structured jet could thus be seen by an off-axis observer with a large viewing angle (e.g., Jin et al. 2017; Lamb & Kobayashi 2017; Lazzati et al. 2017; Xiao et al. 2017; Kathirgamaraju et al. 2018). The low isotropic luminosity ( $\sim 10^{47}$  erg s<sup>-1</sup>) of the prompt emission for GRB 170817A (Goldstein et al. 2017; Zhang et al. 2018b) does support this suggestion. A structured jet has also been favored by other recent theoretical (e.g., Sapountzis & Vlahakis 2014) and numerical (e.g., Aloy et al. 2005; Tchekhovskoy et al. 2008; Komissarov et al. 2010; Murguia-Berthier et al. 2017) studies within the NS–NS merger context. As the jet breaks out of the neutron-rich ‘dynamical ejecta’ ejected during the merger (e.g., Hotokezaka et al. 2013; Rosswog 2013), some ‘lateral structure’ would be developed, which has a lower luminosity than the on-axis relativistic jet.

The prompt emission for GRB 170817A is shown to have two temporal components: a main pulse and a weak tail. The main pulse (−0.26 to 0.57 s) spectrum is well fitted by the cutoff power-law model with the low-energy photon index  $\alpha = -0.61^{+0.34}_{-0.60}$ , while the weak tail (0.95–1.79 s), with  $\sim 1/3$  of the fluence of the main pulse, is

well fitted by a blackbody model (Zhang et al. 2018b, see also Goldstein et al. (2017a)).

The physical origin of the prompt emission of GRB 170817A is unknown. The exponential cutoff on the high-energy end and the relatively hard low-energy photon index (i.e.,  $\alpha = -0.61$  for the time interval between  $-0.26$  and  $0.57$  s) for the main pulse and the dominated blackbody in the weak tail may support a possible photospheric origin of the emission (e.g., Goodman 1986; Paczynski 1986; Abramowicz et al. 1991; Thompson 1994; Mészáros & Rees 2000; Mészáros 2002; Ryde 2004, 2005; Rees & Mészáros 2005; Abdo et al. 2009; Pe’er & Ryde 2011; Lundman et al. 2013; Deng & Zhang 2014; Bégué & Pe’er 2015; Gao & Zhang 2015; Pe’er et al. 2015). On the other hand, the  $\alpha$  index is also consistent with the typical  $\alpha = -2/3$  segment of synchrotron radiation (Rybicki & Lightman 1979). It is therefore interesting to perform detailed modeling of the prompt emission using both photospheric and synchrotron models, especially within the framework of an off-axis structured jet.

This paper is organized as follows. In Section 2, we develop a model of off-axis photosphere emission from a structured jet. Then we apply this model to perform a Markov Chain Monte Carlo (MCMC) fitting to the spectrum of the main pulse of GRB 170817A in Section 3. In Section 4, we apply the MCMC technique to fit the same spectrum using the synchrotron model. Section 5 presents some discussions and the conclusions are drawn in Section 6.

## 2. OFF-AXIS PHOTOSPHERE MODEL IN A STRUCTURED JET

In this section, we present the calculation of the time-integrated photospheric emission spectrum from a structured jet observed by an off-axis observer.

### 2.1. Jet Structure

The jet adopted here is a structured jet with an angle-dependent luminosity (the injected power at the base of the flow) and baryon loading parameter<sup>1</sup> outside a uniform core (e.g., Dai & Gou 2001; Rossi et al. 2002; Zhang & Mészáros 2002a; Kumar & Granot 2003), i.e.,

$$\begin{aligned} L(\theta) &= \frac{L_0}{[(\theta/\theta_{c,L})^{2q} + 1]^{1/2}}, \\ \eta(\theta) &= \frac{\eta_0}{[(\theta/\theta_{c,\Gamma})^{2p} + 1]^{1/2}} + 1.2, \end{aligned} \quad (1)$$

where  $\theta$  is the angle measured from the jet axis,  $\theta_{c,L}$  and  $\theta_{c,\Gamma}$  are the half-opening angles for the luminosity core and the bulk Lorentz factor core ( $\theta_{c,L} = \theta_{c,\Gamma}$  is considered in our calculation),  $L_0$  and  $\eta_0$  are corresponding constant values in the core, respectively,  $q$  and  $p$  describe how the luminosity and the bulk Lorentz factor decrease outside the core. Figure 1 presents the shape of the luminosity and Lorentz factor structures and the best-fit parameters presented in Section 3.

### 2.2. Photosphere Emission Spectrum

<sup>1</sup> Notice that the baryon loading parameter  $\eta$  at the base of the flow is also the bulk Lorentz factor  $\Gamma$  in the saturated acceleration regime.

In the traditional photosphere model, the photospheric radius  $R_{\text{ph}}$  is the radius where the scattering optical depth for a photon moving towards the observer is equal to unity ( $\tau = 1$ ). However, one should realize that wherever there is an electron, a photon has a probability to be scattered there. For an expanding shell, photons can be last-scattered at any position in the shell with a probability depending on the position. This changes the traditional spherical shell photosphere to a probability photosphere discussed by several authors (Pe’er 2008; Beloborodov 2011; Pe’er & Ryde 2011; Lundman et al. 2013; Deng & Zhang 2014). Following the literature, we define a probability function  $P_1(r, \Omega)$  as the probability for a photon being last scattered at the radius  $r$  and angular coordinate  $\Omega$ . This probability function may be calculated by (see Lundman et al. 2013)

$$P_1(r, \Omega) = (1 + \beta)D^2 \times \frac{R_{\text{ph}}}{r^2} \exp\left(-\frac{R_{\text{ph}}}{r}\right), \quad (2)$$

where  $\beta$  is the jet velocity and  $D = [\Gamma(1 - \beta \cdot \cos \theta)]^{-1}$  is the Doppler factor.

In order to obtain the observed spectrum we need to know the probability of the observer-frame photon energy  $E$  when the photon undergoes the last scattering at  $(r, \Omega)$ . This photon energy distribution in the observer frame is determined by that in the co-moving frame and  $E = D(\Omega) \cdot E'$ , where  $E'$  is the co-moving frame photon energy. The photon energy distribution in the local co-moving frame is assumed to be a Planck function with the same temperature as the electron due to the coupling of photons and electrons. Then the photon temperature in the observer frame  $T^{\text{ob}}$  at  $(r, \Omega)$  can be deduced from the plasma temperature  $T'(r, \Omega)$  through  $T^{\text{ob}} = D(\Omega) \cdot T'(r, \Omega)$ . Thus, we can get the distribu-

Log (L) / Log ( $\eta$ )

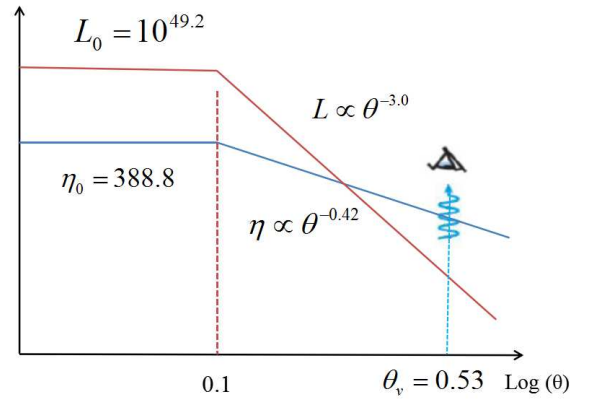


FIG. 1.— Jet structure and viewing angle for our photosphere model fitting of the main pulse spectrum ( $-0.3$  s to  $0.4$  s) of GRB 170817A. For our photosphere model fitting in Section 3, the best-fit values are  $L_0 \sim 10^{49.16}$  erg s $^{-1}$ ,  $\theta_{c,L} \sim 0.11$  rad and  $q \sim 2.99$  for the angular profile of luminosity,  $\eta_0 \sim 388.82$ ,  $\theta_{c,\Gamma} \sim 0.11$  rad and  $p \sim 0.42_{-0.07}^{+0.52}$  for the angular profile of bulk Lorentz factor, and viewing angle  $\theta_v = 0.53$  rad. Thus we get  $L \sim 10^{47}$  erg s $^{-1}$  and  $\Gamma \sim 20$  at the line of sight. For the model calculation in Section 2.3, we take  $L_0 = 10^{50}$  erg s $^{-1}$ ,  $\theta_{c,L} = 0.1$  rad and  $q = 3$  for the angular profile of luminosity, and  $\eta_0 = 200$ ,  $\theta_{c,\Gamma} = 0.1$  rad and  $p = q/4 = 0.75$  for the angular profile of bulk Lorentz factor. The viewing angle  $\theta_v$  is taken to be  $0.8$  rad to get  $L \sim 10^{47}$  erg s $^{-1}$  and  $\Gamma \sim 26$  ( $\eta \sim 40$ ) at the line of sight.

tion function  $P_2(r, \Omega, E)$  of a photon of energy  $E$  and temperature  $T^{ob}$  at  $(r, \Omega)$ , which is described as

$$P_2(r, \Omega, E) = \frac{1}{2.40(kT^{ob}(r, \Omega))^3} \frac{E^2}{\exp(E/kT^{ob}(r, \Omega)) - 1}. \quad (3)$$

When calculating the observed time-integrated spectrum in the following, we adopt the spherical coordinates  $(r, \Omega(\theta_{\text{LOS}}, \phi_{\text{LOS}}))$  corresponding to the line of sight (LOS). The observed time-integrated spectrum is a collection of the photons last scattered at any position  $(r, \theta_{\text{LOS}}, \phi_{\text{LOS}})$  and towards the observer, thus we must know the probability for the last scattering to occur at  $(r, \theta_{\text{LOS}}, \phi_{\text{LOS}})$  as well as the temperature at that location. This probability and temperature are determined by the luminosity and Lorentz factor in the direction  $(\theta_{\text{LOS}}, \phi_{\text{LOS}})$ , which depend completely on the angle  $\theta$  of this direction to the jet axis. If the angle between the jet axis and the LOS (i.e. the viewing angle) is  $\theta_v$ , the corresponding angle  $\theta$  follows

$$\begin{aligned} \theta &= \theta(\theta_{\text{LOS}}, \phi_{\text{LOS}}) \\ &= \arccos[\cos(\theta_{\text{LOS}}) \cos(\theta_v) + \sin(\theta_{\text{LOS}}) \sin(\theta_v) \cos \phi_{\text{LOS}}]. \end{aligned} \quad (4)$$

The time-integrated spectrum can thus be calculated as<sup>2</sup> (see Equation 10 in [Lundman et al. 2013](#))

$$F_E^{ob}(\theta_v) = \frac{1}{4\pi d_L^2} \iint \frac{d\dot{N}_\gamma}{d\Omega} \times P_1(r, \Omega) \times P_2(r, \Omega, E) E d\Omega dr, \quad (5)$$

where  $d\dot{N}_\gamma/d\Omega$  is the photon emission rate per unit solid angle from the base of the outflow ( $r = r_0$ ).

In Equation (5),  $d\dot{N}_\gamma/d\Omega = (L(\Omega)/4\pi)/2.7kT_0(\Omega)$ , where  $L(\Omega)$  is the isotropic luminosity per unit solid angle  $d\Omega$  and  $T_0(\Omega) = (L(\Omega)/4\pi r_0^2 ac)^{1/4}$  is the temperature at the base of the outflow per unit solid angle  $d\Omega$ . As a result,  $d\dot{N}_\gamma/d\Omega$  is angle-dependent.

Since the typical luminosity may be low for a SGRB with rapid decrease of luminosity in the lateral direction, the photosphere radius  $R_{\text{ph}}$  where the photons being last-scattered may be smaller than the saturation radius for jet acceleration  $R_s = \eta(\theta) \cdot r_0$ . We therefore must judge whether the acceleration is saturated ( $R_{\text{ph}} > R_s$ ) in each unit solid angle  $d\Omega$  by calculating  $R_{\text{ph}}$  based on the assumption of saturation, and then deal with them for the calculations of  $P_1$  and  $P_2$  separately. Notice that we have assumed a pure fireball here for simplicity. In principle, the outflow can be “hybrid” with an important contribution from a Poynting flux. The dynamics of such a scenario is more complicated, but the predicted photosphere spectrum would not be much different from the pure fireball case, even though the required parameters would be somewhat different. For a detailed treatment of a hybrid outflow, see [Gao & Zhang \(2015\)](#).

For the saturated case,  $R_{\text{ph}}$  is given by

$$R_{\text{ph}} = \frac{1}{(1 + \beta)\beta\eta^2(\theta)} \frac{\sigma_T}{m_p c} \frac{L(\theta)}{4\pi c^2 \eta(\theta)}, \quad (6)$$

<sup>2</sup> Notice that [Deng & Zhang \(2014\)](#) provided a two-dimensional last scattering probability function  $P(r, \Omega)$ . We adopt the separated probability function  $P_1$  in this paper, since it is more easily generalized to structured jets and MCMC fitting.

where  $\sigma_T$  is the Thompson cross-section, the Doppler factor is  $D = [\eta(\theta) \cdot (1 - \beta(\theta) \cdot \cos \theta_{\text{LOS}})]^{-1}$ , the observer-frame temperature is  $T^{ob} = D(\Omega) \cdot T'(r, \Omega)$ , and the comoving temperature  $T'(r, \Omega)$  is

$$T'(r, \Omega) = \begin{cases} \frac{T_0(\Omega)}{2\eta(\Omega)}, & r < R_s(\Omega) < R_{\text{ph}}(\Omega) \\ \frac{T_0(\Omega) \cdot [r/R_s(\Omega)]^{-2/3}}{2\eta(\Omega)}, & R_s(\Omega) < r < R_{\text{ph}}(\Omega) \\ \frac{T_0(\Omega) \cdot [R_{\text{ph}}(\Omega)/R_s(\Omega)]^{-2/3}}{2\eta(\Omega)}, & R_s(\Omega) < R_{\text{ph}}(\Omega) < r \end{cases} \quad (7)$$

For the unsaturated case,  $R_{\text{ph}}$  is calculated by

$$R_{\text{ph}} = \left[ \frac{\sigma_T}{6m_p c} \frac{L(\theta)}{4\pi c^2 \eta(\theta)} r_0^2 \right]^{1/3}. \quad (8)$$

In this case, the Lorentz factor at the photosphere and the corresponding Doppler factor are given by  $\Gamma(\theta) = R_{\text{ph}}(\theta)/r_0$  and  $D = [\Gamma(\theta) \cdot (1 - \beta(\theta) \cdot \cos \theta_{\text{LOS}})]^{-1}$ , respectively, and the comoving temperature is

$$T'(r, \Omega) = T_0(\Omega)/[2\Gamma(\Omega)]. \quad (9)$$

To calculate the time-resolved spectra, we add a  $\delta$ -function  $\delta(t - ru/\beta c)$  to Equation (5), where  $u = (1 - \beta(\theta) \cdot \cos \theta_{\text{LOS}})$ . One then has

$$\begin{aligned} F_E^{ob}(\theta_v, t) &= \frac{1}{4\pi d_L^2} \iint \frac{d\dot{N}_\gamma}{d\Omega} \times P_1(r, \Omega) \times P_2(r, \Omega, E) \\ &\times \delta(t - \frac{ru}{\beta c}) E d\Omega dr. \end{aligned} \quad (10)$$

With the above analysis, we can derive the time-resolved spectra for impulsive injection of energy and the time-integrated spectrum for continuous long-duration energy injection. For a realistic SGRB the duration for energy injection from the central engine is long ( $\sim 1$  s), as manifested by its observed duration( $T_{90}$ ).

### 2.3. Calculated Spectrum

The parameters of the jet structure and the viewing angle  $\theta_v$  adopted in our calculation are close to the best-fit values shown in Figure 1. We set the luminosity at the line of sight to be  $\sim 10^{47}$  erg s<sup>-1</sup> to match the observation of GRB 170817A. According to SGRBs data, typically one has  $L_0 \sim 10^{50}$  erg s<sup>-1</sup> and  $\theta_{c,L} \simeq 6^\circ - 16^\circ$  ([Fong et al. 2015](#); [Ghirlanda et al. 2016](#)). For a power-law structured jet, the parameter  $q$  may be obtained through the luminosity dependence of local event rate density  $\rho_0(> L)$  of SGRBs (e.g. [Zhang & Mészáros 2002a](#)). Since  $\rho_0(> L) \propto L^{-\lambda}$  ( $\lambda \sim 0.7$ , [Sun et al. 2015](#)) and  $\rho_0(> L) \propto \Omega(> E) \simeq \pi\theta^2$ , the isotropic-equivalent luminosity  $L \propto \theta^{-2/\lambda} \propto \theta^{-q}$ , then  $q \simeq 2.86$ . Thus we take  $L_0 = 10^{50}$  erg s<sup>-1</sup>,  $\theta_{c,L} = 0.1$  rad, and  $q = 3$  here. Meanwhile we take the viewing angle  $\theta_v$  as 0.8 rad to match the luminosity mentioned above. With this viewing angle and other parameters we can obtain the approximate model spectrum and thus check whether we can perform a more detailed MCMC fit for the spectrum of GRB 170817A. Also by comparing with the best-fit parameters (see Sect.3) and the model spectrum for those best-fit parameters (shown in the bottom left panel of Fig.3), we can acquire the degree of the change for the parameters corresponding to different model spectra. As

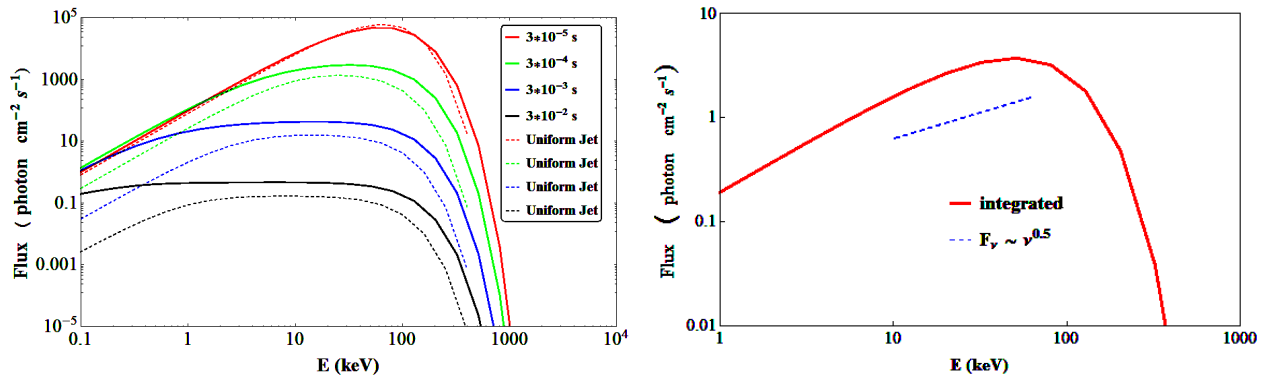


FIG. 2.— The calculated time-resolved spectra and the time-integrated spectrum. Left panel: the solid lines show the time-resolved spectra calculated with the parameters of the structured jet described in the text. The dashed lines show the time-resolved spectra calculated in Deng & Zhang (2014) for a uniform jet. For the case of a structured jet, the low-energy flux at later times is greatly boosted. Right panel: the time-integrated spectrum for the structured jet. The spectrum has a much softer low-energy photon index  $\alpha \sim -0.5$  than blackbody and an exponential high-energy cutoff, which are close to the empirical fitting results of the main pulse spectrum of GRB 170817A.

for the bulk Lorentz factor, we let the value along the line of sight to be in the range of  $(20 - 40)$  in order to match the peak energy ( $\sim 100$  keV) of the observed spectrum. In addition, we take  $\eta \propto L^{1/4}$  according to the statistical results of a large sample of GRBs (Liang et al. 2010; Lü et al. 2012). Finally, we adopt  $\eta_0 = 200$ ,  $\theta_{c,\Gamma} = 0.1$  rad, and  $p = q/4 = 0.75$ .

The left panel of Figure 2 shows the calculated time-resolved spectra and the right panel is the time-integrated spectrum<sup>3</sup>. Comparing the time-resolved spectra of a structured jet (solid lines in the left panel) and those of a uniform jet (dashed lines in the left panel), we can see that the low-energy power-law segment below the peak energy  $E_p$  is softer than the uniform jet case, and the total fluxes are also higher. This is because the low-energy emission has a significant contribution from the high latitudes with respect to the line of sight in the directions with smaller angles from the jet axis where intrinsic luminosity is high but Doppler factor is low.

The low-energy photon index is  $\alpha \sim -0.5$  for the time-integrated spectrum in the right panel. This is much softer than the case of the uniform jet ( $\alpha \sim 0.5$ , Deng & Zhang 2014). The origin of such a difference is again due to the enhanced near-axis high-latitude emission, likely caused by structures or change in Lorentz factor and luminosity. There are two effects here. First, the luminosity structure enhances the near-axis high-latitude emission. Second, the Lorentz factor structure also allows emission from some directions to become unsaturated, which would also contribute to the enhancement. The predicted low-energy photon index ( $\alpha \sim -0.5$ ) of this model as well as the exponential cutoff on the high-energy end are consistent with the time-integrated spectrum of GRB 170817A, which can be empirically fitted by a cutoff power-law model with the low-energy photon index  $\alpha \sim -0.6$  (Goldstein et al. 2017; Zhang et al. 2018b). This encourages us to perform a more detailed MCMC fit of the data using our off-axis photospheric emission model from a structured jet.

<sup>3</sup> When calculating results in Fig.2 we do not make use of the best-fit parameters in Sect.3 but rather use the example parameters, since the spectrum for the best-fit parameters is presented in the bottom left panel of Fig.3.

### 3. SPECTRAL FITTING OF GRB 170817A WITH THE OFF-AXIS PHOTOSPHERE MODEL

GRB 170817A was detected by *Fermi*-GBM and INTEGRAL SPI-ACS, with the luminosity distance of  $\simeq 40$  Mpc (Abbott et al. 2017b). The analysis of the *Fermi*-GBM data showed two components: a main pulse from  $T_0 - 0.26$  s to  $T_0 + 0.57$  s and a weak tail extending from  $T_0 + 0.95$  s to  $T_0 + 1.79$  s (Goldstein et al. 2017; Zhang et al. 2018b). In this work we choose the interval (i.e., between  $T_0 - 0.3$  s to  $T_0 + 0.4$  s) with the most significant emission to perform the model fitting. We analyze the GBM Time Tagged Event (TTE) data from detectors NaI 1, NaI 2 and BGO 0. We fit the spectra using our photosphere model described in Section 2, with McSpecFit package which accepts flexible user-defined spectral model (Zhang et al. 2016a). A fit with the empirical cutoff power-law function was first performed. The spectrum of this interval is best-fitted by the cutoff power-law model with the low-energy photon index of  $-0.62^{+0.49}_{-0.54}$ , peak energy  $E_p = 145^{+140}_{-26}$  keV, and the time-averaged flux of  $(2.5^{+1.8}_{-1.0}) \times 10^{-7}$  erg cm $^{-2}$  s $^{-1}$ . The weak tail between  $T_0 + 0.95$  s and  $T_0 + 1.79$  s, with 34% the fluence of the main pulse, is best fitted by a blackbody spectrum with  $kT = 11.3^{+3.8}_{-2.4}$  keV (Goldstein et al. 2017; Zhang et al. 2018b).

A comparison between our photosphere model fitting and the cutoff power-law model fitting is shown in Figure 3. The best fitting parameters are presented in Table 1 and also shown in Figure 1. It is apparent that our photosphere model can fit the data as well as the cutoff power-law model, with a PGSTAT/dof = 260.9/357 = 0.73 (260.1/363 = 0.72 for the cutoff power-law model). In addition, the residuals do not show any marked trends.

Parameter constraints of our photosphere model are illustrated in Figure 4. The best-fit values for the luminosity profile,  $L_0 \sim 10^{49.16}$  erg s $^{-1}$ ,  $\theta_{c,L} \sim 0.11$  rad and  $q \sim 2.99$  are consistent with the reasonable values of  $L_0 = 10^{50}$  erg s $^{-1}$ ,  $\theta_{c,L} = 0.1$  rad and  $q = 3$  (Fong et al. 2015; Sun et al. 2015; Ghirlanda et al. 2016). Also, the best-fit values for the bulk Lorentz factor profile,  $\eta_0 \sim 388.82^{+82.2}_{-62.9}$  and  $p \sim 0.42^{+0.52}_{-0.07}$  are close to the reasonable values of  $\eta_0 = 200$  and  $p = 0.75$ . The best-fit viewing angle  $\theta_v \sim 0.53^{+0.08}_{-0.17}$  rad falls into the reasonable range



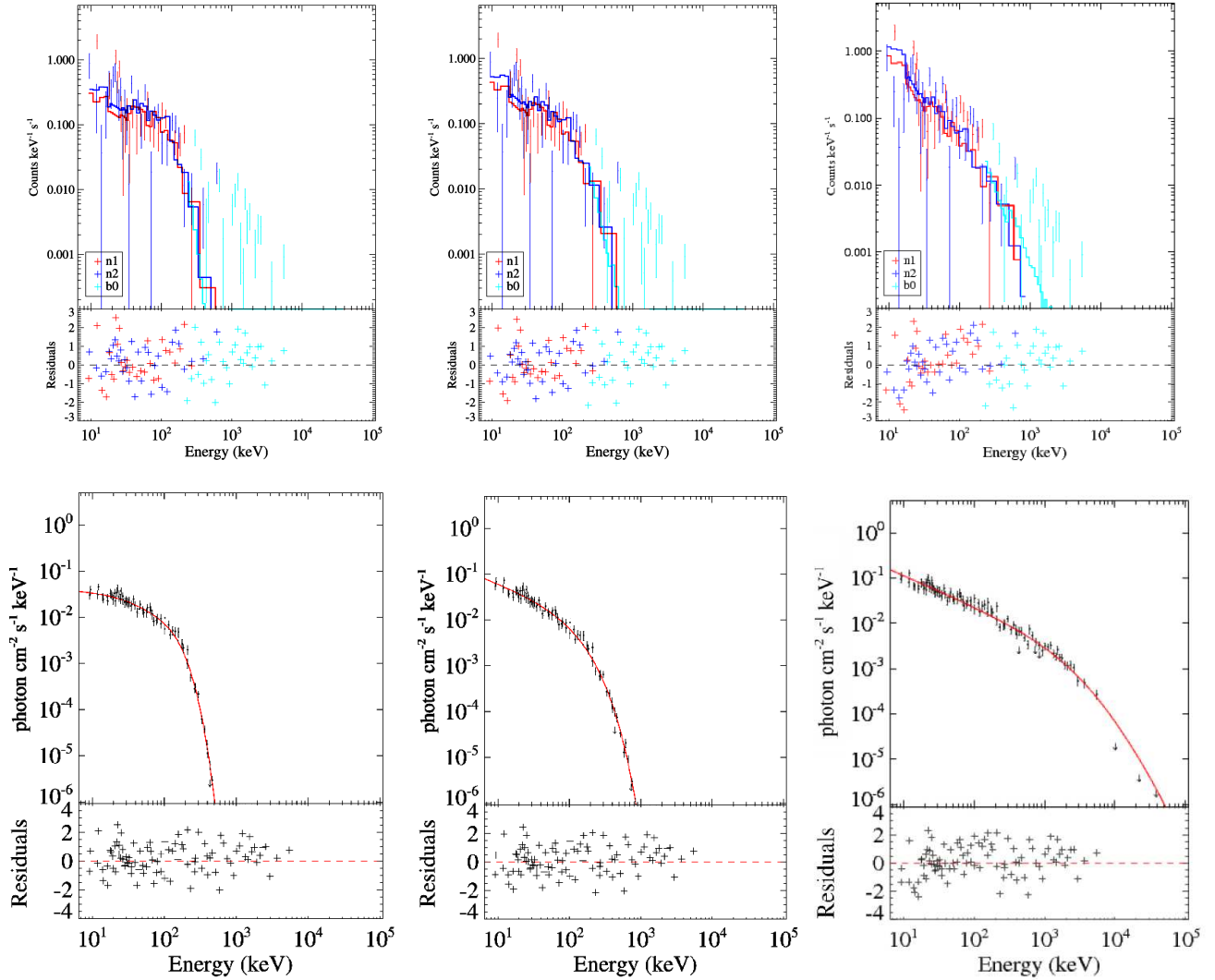


FIG. 3.— Comparisons among our photosphere model fitting, the cutoff power-law model fitting and the synchrotron model fitting for the time-integrated spectrum between  $-0.3$  s and  $0.4$  s. Top panels: observed count spectrum and model count spectrum for our photosphere model fitting (top left), the cutoff power-law model fitting (top middle) and the synchrotron model fitting (top right). Bottom panels: theoretical photon spectrum (red line) and observed photon flux (data points, which are obtained by using the instrument responses to de-convolve the observed count spectrum) for our photosphere model fitting (bottom left), the cutoff power-law model fitting (bottom middle) and the synchrotron model fitting (bottom right). The legends of “n1, n2, b0” in the top panels indicate the two Thallium activated Sodium Iodide crystal detectors, named as NaI n1, NaI n2, and one Bismuth Germanate crystal detector, named as BGO b0.

( $0.65 - 0.72$  rad in [Granot et al. 2017b](#) and  $0.7$  rad in [Gottlieb et al. 2017](#)). The observed luminosity<sup>4</sup> at the line of sight is  $L \simeq 1.3 \times 10^{47}$  erg s<sup>-1</sup>, which is consistent with the data ([Goldstein et al. 2017](#); [Zhang et al. 2018b](#)). The best-fit initial radius  $r_0$  for acceleration is  $\sim 10^{7.46}$  cm. We find that the acceleration is unsaturated ( $R_{\text{ph}} \sim 4.9 \times 10^8$  cm and  $R_s \sim 5 \times 10^9$  cm) at the line of sight and the actual Lorentz factor<sup>5</sup> at the line of sight is  $\Gamma \sim 17$ .

<sup>4</sup> Since the injected photons are almost emitted at the photosphere, the ratio of the observed temperature there to the temperature at the base  $T_0$  represents the efficiency. In the saturated case, the efficiency is  $(R_s/R_{\text{ph}})^{2/3}$ ; while in the unsaturated case the efficiency is  $\sim 1$ , which turns out to be the actual case.

<sup>5</sup> Notice that [Zou et al. \(2018\)](#) got a Lorentz factor  $\Gamma \sim 13.4$  for the case of an off beaming relativistic jet.

The best-fit initial acceleration radius  $r_0$  is  $\sim 10^{7.46}$  cm. [Bégué et al. \(2017\)](#) gave an estimate of the  $r_0$  based on the fitted peak energy and flux of a single black-body in the observed spectrum (with the existence of a non-thermal component) using the method of [Pe’er et al. \(2007\)](#), and found that  $r_0$  is too small ( $3 \times 10^6$  cm, close to the innermost stable circular orbit of a black hole with  $3 M_\odot$ ) to justify the photosphere model. This seems to be in contradiction with our result. We’d like to point out two significant differences between our photosphere model and theirs. First, the method to estimate the  $r_0$  given in [Pe’er et al. \(2007\)](#) is only valid for the case of saturated acceleration ( $R_{\text{ph}} > R_s$ ). Thus, the unreasonable low  $r_0$  only means that the photosphere model for saturated acceleration is unable to explain the data well. There is no conflict for our result (large  $r_0$ ) since we

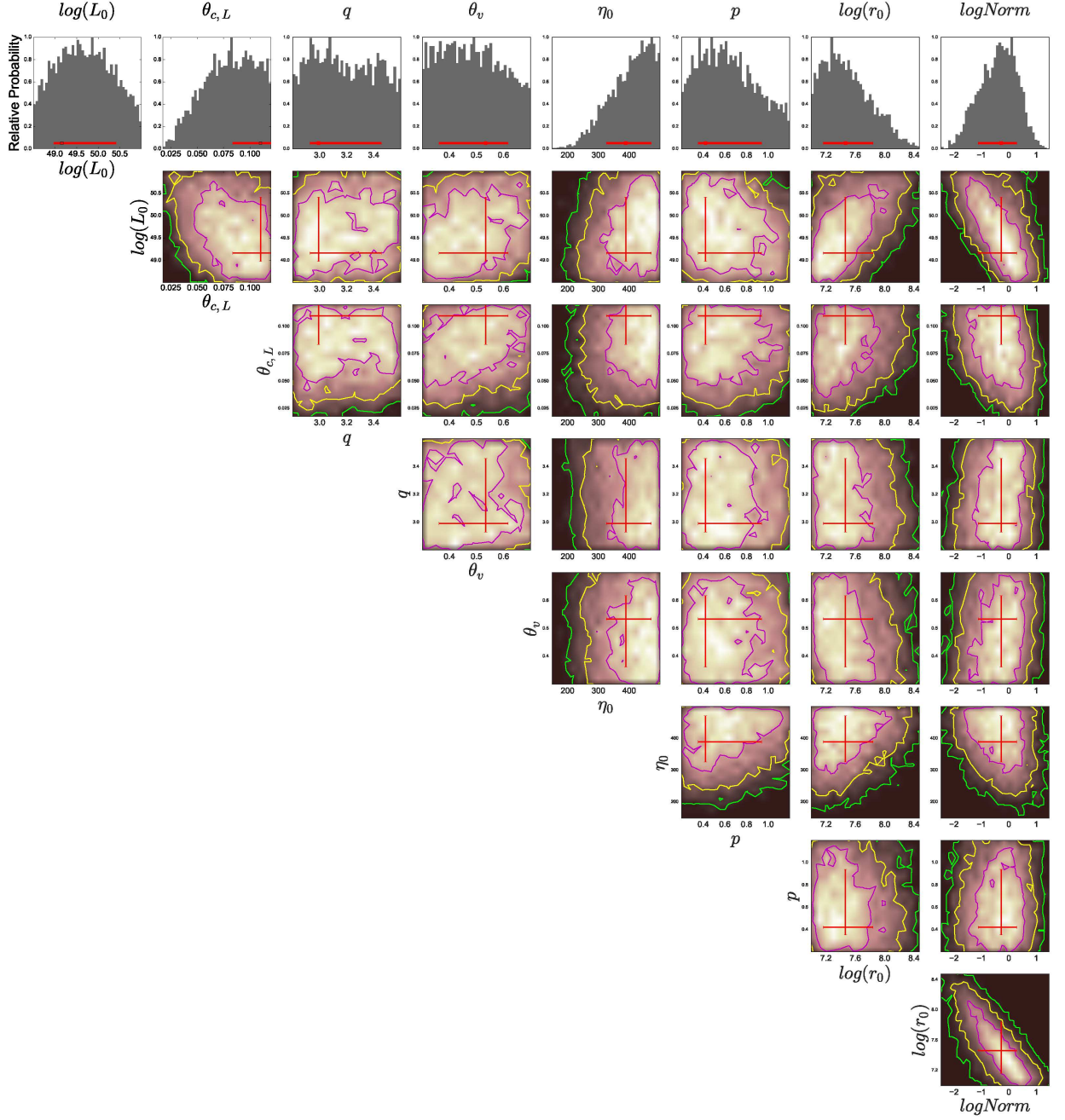


FIG. 4.— Parameter constraints of our photosphere model fitting for the time-integrated spectrum between  $-0.3$  s and  $0.4$  s. Histograms and contours illustrate the likelihood map. Red crosses show the best-fit values and 1-sigma error bars.

are in the unsaturated regime. Second, their method relies on the assumption of a single blackbody contributed within a small cone along the line of sight, and an additional non-thermal component is needed to account for the observed spectrum. Our model, on the other hand, invokes a structured jet so that emission from high latitudes (relative to the LOS) is included in the calculation. The resulting spectrum is naturally a multi-color blackbody, which can account for the observed spectrum well without the need of introducing a non-thermal component. As a result, our best-fit value  $r_0$  is justified.

Furthermore, since the acceleration is in the unsaturated regime ( $R_{\text{ph}} < R_s$ ) along the line of sight, adiabatic cooling is not involved (unlike the saturated case, see Equation 7 and Equation 9). As a result, the observed peak energy should be much higher than that in the saturated case for the same isotropic energy. This seems to be true for this burst (see Figure 3 in Zhang et al. 2018b).

TABLE 1  
SPECTRAL FITTING PARAMETERS USING OFF-AXIS PHOTOSPHERE MODEL.

| Parameters                  | GRB 170817A                |
|-----------------------------|----------------------------|
| $\log L_0$ (erg s $^{-1}$ ) | $49.16^{+1.25}_{-0.18}$    |
| $\theta_{c,L}$ (rad)        | $0.11^{+0.01}_{-0.02}$     |
| $q$                         | $2.99^{+0.46}_{-0.06}$     |
| $\theta_v$ (rad)            | $0.53^{+0.08}_{-0.17}$     |
| $\eta_0$                    | $388.82^{+82.21}_{-62.90}$ |
| $p$                         | $0.42^{+0.52}_{-0.07}$     |
| $\log r_0$ (cm)             | $7.46^{+0.37}_{-0.30}$     |
| $\log \text{Norm}$          | $0.28^{+0.58}_{-0.84}$     |

#### 4. SYNCHROTRON MODEL FITTING

Synchrotron radiation from accelerated electrons in an optically thin region is another promising radiation mechanism for GRB prompt emissions. In this section, we apply a synchrotron radiation model to fit the spectra of GRB 170817A. To explain the hard low-energy spectrum, Uhm & Zhang (2014) proposed that fast-cooling electrons in a decaying magnetic field can form a hard electron distribution, which results in a hard radiation spectrum (also see Derishev 2007). Since the observed spectral index is much harder than the standard fast-cooling spectrum ( $\alpha = -1.5$ ) (Sari et al. 1998), we adopt the scenario of synchrotron radiation in a decaying magnetic field (Uhm & Zhang 2014) in our modeling.

Synchrotron radiation can in principle originate from internal shocks (Rees & Mészáros 1994) or a magnetic reconnection region (e.g. triggered by internal-collision-induced magnetic reconnection and turbulence, IC-MART) (Zhang & Yan 2011). The former is relevant for a matter-dominated fireball, which should be accompanied by a bright photosphere component. If one interprets the first pulse of GRB 170817A as due to the synchrotron radiation, the lack of an earlier photosphere component suggests that the outflow is likely Poynting-flux-dominated, so that the ICMART model may be more relevant.

Relativistic magnetic reconnection and the shock process are believed to be able to accelerate non-thermal particles and develop a power-law spectrum of the particle acceleration (see e.g., Guo et al. 2014, 2016; Sironi & Spitkovsky 2014; Ardaneh et al. 2015). We assume that a group of electrons, which obey a power-law distribution, i.e.,  $Q(\gamma'_e, t') = Q_0(t')(\gamma'_e/\gamma'_m)^{-p}$  for  $\gamma'_e > \gamma'_m$ , are injected in the relativistically moving shell of Lorentz factor  $\Gamma$ . Here,  $Q_0$  is related to the injection rate  $N'_{\text{inj}}$  by  $N'_{\text{inj}} = \int_{\gamma'_m}^{\gamma'_{\text{max}}} Q(\gamma'_e, t') d\gamma'_e$ , where  $\gamma'_{\text{max}}$  is the maximum Lorentz factor of electrons. For an electron of  $\gamma'_e$ , it would lose energy by synchrotron radiation, of which the cooling rate is

$$\dot{\gamma}'_e = -\frac{\sigma_T B'^2 \gamma'^2_e}{6\pi m_e c}, \quad (11)$$

where  $B'$  is the magnetic field in the co-moving frame. Recent studies reveal that synchrotron self-Compton (SSC) cooling may also play an important role in shaping the electron energy distribution (Bošnjak et al. 2009; Daigne et al. 2011; Geng et al. 2018). However, the effect of SSC cooling on the resulting spectra is similar to that of decaying magnetic fields. Here we do not include it for simplicity in our calculations and this would not markedly impact our main conclusions. Denoting the instantaneous spectrum of electrons as  $\frac{dN_e}{d\gamma'_e}$ , one can obtain it by solving the continuity equation in energy space (Longair 2011)

$$\frac{\partial}{\partial t'} \left( \frac{dN_e}{d\gamma'_e} \right) + \frac{\partial}{\partial \gamma'_e} \left[ \dot{\gamma}'_e \left( \frac{dN_e}{d\gamma'_e} \right) \right] = Q(\gamma'_e, t'). \quad (12)$$

Considering a conical jet, the co-moving magnetic field in the jet would decay with radius as

$$B' = B'_0 \left( \frac{R}{R_0} \right)^{-1}, \quad (13)$$

where  $B'_0$  is the magnetic strength at  $R_0$ , and  $R_0$  is the radius where the jet begins to emit the first photon observed by us. In our modeling, we take  $R_0 = 2\Gamma^2 c \times 1$  s, and denote observer-frame time since the first electron injection as  $\hat{t}$  (in units of s) for an emission episode. We further introduce a parameter  $t_{\text{off}}$  to describe when the injection of electrons is turned off in the observer frame. Therefore, seven parameters in total are left free, i.e.,  $\Gamma$ ,  $\gamma'_m$ ,  $B'_0$ ,  $p$ ,  $N'_{\text{inj}}$ ,  $t_{\text{off}}$  and  $\hat{t}$ . Unlike the calculation method for spectra adopted in Section 2, we only consider the emission from the region just near the LOS and treat this small region as a uniform jet. So relevant parameters in our calculation describe properties of the region near the LOS, rather than those of the jet axis. This treatment enables us to simplify the calculation and focus on properties of the region near the LOS. Unlike photosphere emission for which one has considered the shape of the last-scattering surface which could be noticeably different for a structured jet, the synchrotron model is not affected by the jet structure if the Lorentz factor along the LOS is large enough (e.g. Zhang & Mészáros 2002a). This is valid for our case (our best-fit  $\Gamma \sim 96$  along the LOS, so our simplification does not impact final results significantly).

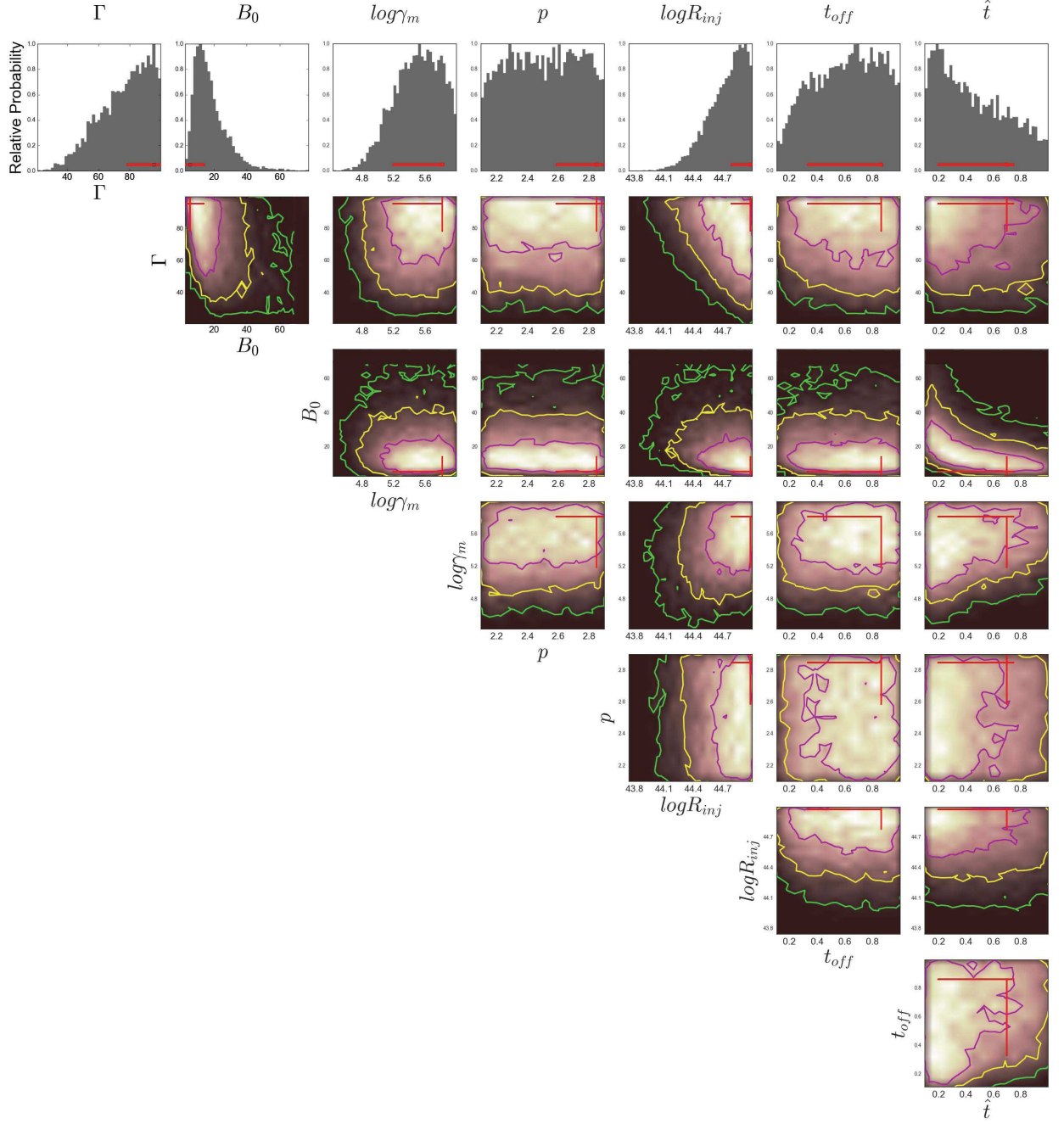


FIG. 5.— Parameter constraints of the synchrotron model fitting for the time-integrated spectrum between  $-0.3$  s and  $0.4$  s.



We fit the spectra by interpolating our synchrotron model into the McSpecFit package (also see Zhang et al. 2018a,b for details), and the fitting results are shown in Table 2 and Figure 5, with a PGSTAT/dof = 269.4/359. Compared with the PGSTAT/dof = 260.9/357 for the photosphere model, the PGSTAT/dof for the synchrotron model is slightly larger. However, this small difference could not help to prefer one model over the other.

One can perform a self-consistency check of the synchrotron model parameters. The GRB emission is delayed by  $\Delta t \sim 1.7$  s with respect to the gravitational wave merger time (Abbott et al. 2017b; Zhang et al. 2018b). If one assumes that the jet is launched right after the merger, the distance the jet traveled at the time of magnetic dissipation is  $R_{\text{GRB}} \sim \Gamma^2 c \Delta t \sim 4.7 \times 10^{14}$  cm. Given the observed luminosity  $L \sim 10^{47}$  erg s $^{-1}$ , the co-moving magnetic field in the emission region may be estimated as (e.g. Zhang & Mészáros 2002b)  $B' \leq (2L/cR_{\text{GRB}}^2)^{1/2}/\Gamma \sim 58$  G. The best-fit parameter falls within this range, suggesting the consistency of the model.

TABLE 2  
SPECTRAL FITTING PARAMETERS USING SYNCHROTRON MODEL.

| Parameters                         | GRB 170817A              |
|------------------------------------|--------------------------|
| $\Gamma$                           | $95.57^{+4.43}_{-17.51}$ |
| $B'_0$ (G)                         | $5.45^{+8.96}_{-2.76}$   |
| $\log \gamma'_m$                   | $5.82^{+0.001}_{-0.63}$  |
| $p$                                | $2.85^{+0.05}_{-0.26}$   |
| $\log R_{\text{inj}}$ (s $^{-1}$ ) | $44.98^{+0.02}_{-0.20}$  |
| $t_{\text{off}}$ (s)               | $0.86^{+0.01}_{-0.54}$   |
| $\hat{t}$ (s)                      | $0.70^{+0.05}_{-0.51}$   |

Our results suggest that the synchrotron model can also give a reasonable interpretation to the first pulse of the prompt emission of GRB 170817A. More complicated effects such as SSC (Geng et al. 2018) and slow heating/acceleration for electrons (Xu & Zhang 2017; Xu et al. 2018) have not been considered in our calculation. However, since these effects also tend to harden the spectrum, including them would also give a reasonable interpretation to the data, even though the best-fit parameters may be somewhat changed.

## 5. DISCUSSION

### 5.1. The Blackbody in the Weak Tail

The spectrum of the weak tail emission of GRB 170817A is consistent with being a blackbody. Within our structured jet photosphere model, this may be interpreted as the transition from a structured jet to a roughly uniform jet at late times or the change of Lorentz factor and luminosity such that the contributions to observed flux from high latitudes are weakened. The softer peak energy is a natural result from the decrease of the luminosity and the Lorentz factor at late times. According to the best-fit results for the main pulse above, we have  $L \sim 10^{47}$  erg s $^{-1}$ ,  $\eta \sim 50 - 150$  at the line of sight. Thus for the weak tail with  $L \sim 0.3 \times 10^{47}$  erg s $^{-1}$ , if the bulk Lorentz factor  $\eta \sim 20$  (saturated acceleration with

$R_{\text{ph}} \sim 3.3 \times 10^9$  cm and  $R_s \sim 5.8 \times 10^8$  cm), we may get a blackbody spectrum with  $kT = 11.3^{+3.8}_{-2.4}$  keV. One should note that these are the average values within the entire duration of the weak tail.

Within the synchrotron model, the blackbody tail emission should be attributed to a different mechanism. One may suppose that a successful structured jet breaks out to make the first pulse via synchrotron, and the more isotropic component breaks out the cocoon later to make the second thermal tail. Therefore, it is unable to rule out the synchrotron model based on the existence of the thermal tail.

### 5.2. The Time Delay between the GW Signal and the SGRB

The  $\gamma$ -ray emission onset of GRB 170817A has a delay of  $\Delta t = 1.74 \pm 0.05$  s relative to the GW chirp signal (Abbott et al. 2017b). Under the framework of photosphere model, some additional mechanism is required to account for such a delay. For instance, this delay may be attributed to the existence of a short-lived (thmns  $\lesssim 1$  s) hypermassive NS (HMNS) after the NS–NS merger, and the jet is launched only after the hypermassive NS collapses into a black hole (e.g. Granot et al. 2017a). Such type of the NS–NS merger remnant is supported by previous numerical studies (e.g., Rosswog & Davies 2002; Rosswog et al. 2003). The delay onset of a relativistic jet relative to the merger is also required by the cocoon model (e.g. Gottlieb et al. 2017). After launching, the relativistic jet needs to break through the dynamical ejecta (e.g., Hotokezaka et al. 2013; Rosswog 2013) and/or neutrino driven wind, causing another time delay that could be a large fraction of a second (e.g., Moharana & Piran 2017; Nakar & Piran 2017).

Within the photosphere model, if one assumes  $\Gamma \approx 2 - 3$  along the line of sight for the structured jet, the observed delay can be well explained without introducing an extra delay for the onset of the jet. In this case, however, the photosphere temperature is too low to explain the observed  $E_p$ . One needs to introduce some sub-photospheric dissipative processes to boost up  $E_p$  through Comptonization (Rees & Mészáros 2005; Giannios 2006; Bégue & Pe'er 2015; Vurm & Beloborodov 2016).

Within the synchrotron model, one does not need to invoke such a delayed launch of jet with respect to the merger time. The delay can be accounted for by the time scale when the relativistic jet reaches the dissipation radius. It is intriguing that both the duration of the burst and the delay time are of the same order. Within the synchrotron model, both time scales are related to  $R_{\text{GRB}}/c\Gamma^2$ , and therefore are comparable (Zhang et al. 2018b).

### 5.3. Comparison with the Cocoon Emission Model

Using the cocoon shock breakout to explain the  $\gamma$ -ray emission of GRB 170817A has been proposed lately (e.g., Gottlieb et al. 2017; Kasliwal et al. 2017; Bromberg et al. 2018). A delayed launch of the jet after the merger is needed to explain the data. In order to explain the soft low-energy photon index of the main pulse spectrum, both the cocoon shock breakout and our scenario attribute the soft emission below  $E_p$  to the su-

perposition of a series of blackbody with different temperatures. The significant difference between their model and ours is the origin of low luminosity. In our model, the low luminosity is caused by the low luminosity of the structured jet along the line of sight, since we think that the jet may have a decreasing luminosity with angle and the viewing angle is large. The low luminosity of the cocoon shock breakout model arises from the low mass (thus low internal energy,  $m_{\text{tail}} \sim 4 \times 10^{-7} M_{\odot}$ ) of the fast ejecta tail which emits  $\gamma$ -ray photons with a small Lorentz factor  $\Gamma_s \approx 2 - 3$ .

It is worth emphasizing that GRB 170817A appears a natural extension of short GRBs to the low-luminosity regime. The duration ( $T_{90}$ ) and the peak energy of GRB 170817A are similar to a group of short GRBs (Lu et al. 2017; Zhang et al. 2018b). The average low-energy photon index ( $\alpha \sim -0.69$ , Burgess et al. 2017; Lu et al. 2017) for the complete short GRBs sample of *Fermi* GBM is close to the low-energy photon index ( $\alpha \sim -0.62$ ) of this burst. The SGRB event rate density above a much lower luminosity threshold ( $\sim 10^{47}$  erg s $^{-1}$ ), obtained by including GRB 170817A, is found to be consistent with the extension of the PL distribution for the normal SGRBs with higher luminosities (Zhang et al. 2018b). All these suggest that GRB 170817A may not have a very different origin from other short GRBs. The radiation mechanism for GRB 170817A is likely to be the same as that of other short GRBs with high luminosity. We believe that photosphere emission or synchrotron radiation from a structured jet with a large viewing angle is a natural explanation to the prompt emission data of GRB 170817A, and the cocoon model may not be needed to account for the data<sup>6</sup>. It has been suggested that the recent brightening of radio and X-ray fluxes is consistent with the prediction of the cocoon model (Kasliwal et al. 2017). On the other hand, the structured jet model can also explain the same data available so far (Lazzati et al. 2017b) as well as the late-time optical afterglow (Lyman et al. 2018).

## 6. CONCLUSIONS

As the first short GRB detected to be associated with a NS–NS merger event, GRB 170817A carries important clues to unveil the underlying physics of SGRBs, including jet launching, interaction with the dynamical ejecta, energy dissipation mechanism, and radiation mechanism. The prompt emission data can be used to constrain these mechanisms.

In this paper, we focus on the spectral data of the first emission episode of GRB 170817A, and explore two models to account for the observed data. We find that both models can give reasonable fit to the data. In the first model, we developed a photosphere model in a structured jet. We found that the emission from the part closer to the jet axis can enhance the low-energy component of the spectrum, resulting in a softer low-energy photon index ( $\alpha \sim -0.5$ ) which is consistent with the observation ( $\alpha \sim -0.6$ ). We performed a MCMC fit of the spectrum

from  $T_0 - 0.3$  s to  $T_0 + 0.4$  s using our model, and found that our model can give a comparable fit to the best-fit empirical model (the cutoff power-law model). The best-fit parameters are consistent with the results from some statistic works for SGRBs. In the second model, we consider synchrotron radiation in an optically thin region with the jet expanding with a decaying magnetic field strength. This model also gives a reasonable fit to the data, even though a higher Lorentz factor along the line of sight is needed.

GRB 170817A is observed to be delayed from GW170817 by  $\sim 1.7$  s. Within the photosphere model, one needs to introduce a delay of the launch of the jet after the merger. Such a requirement is also needed by the cocoon shock break model. The synchrotron model does not demand such a delay time.

Bégué et al. (2017) discussed whether the typical emission models of synchrotron radiation and photospheric emission for structured and top-hat jets can explain the prompt emission of GRB 170817A, and found that these models are particularly challenging. They then proposed that the standard models for SGRBs need to be modified. We reached an opposite conclusion by introducing a structured jet so that the observed spectrum is intrinsically multi-color blackbody. Another difference is that jet acceleration is in the unsaturated regime. As we have shown, the photosphere model can give a very good fit to the data. For synchrotron radiation, we reached a set of best-fit parameters which are not unreasonable, in contrast to the conclusion of Bégué et al. (2017). We therefore conclude that both mechanisms are not ruled out by the data, and that the standard GRB mechanism (with a large viewing angle to a structured jet) can account for the prompt emission data of GRB 170817A without the need to invoke a different mechanism, e.g. cocoon shock breakout.

We thank the referee for helpful suggestions. We acknowledge the use of the public data from the *Fermi* data archives. This work is supported by the National Basic Research Program (“973” Program) of China (Grant No. 2014CB845800), the National Natural Science Foundation of China (Grant Nos. 11725314, 11673068, 11433009, 11543005, 11603076, 11573014, 11533003, 11473012, 11722324, 11603003, 11633001 and 11690024), the Youth Innovation Promotion Association (2011231 and 2017366), the Key Research Program of Frontier Sciences (QYZDB-SSW-SYS005), the Strategic Priority Research Program “Multi-waveband gravitational wave Universe” (Grant No. XDB23000000) of the Chinese Academy of Sciences, and the Natural Science Foundation of Jiangsu Province (Grant No. BK20161096). JJG is supported by the National Postdoctoral Program for Innovative Talents (Grant No. BX201700115) and China Postdoctoral Science Foundation funded project (Grant No. 2017M620199). BBZ acknowledge the support from the National Thousand Young Talents program of China.

## REFERENCES

<sup>6</sup> We stress that the cocoon may still exist in our models. But for our scenarios the outflow from the central engine can break out the cocoon quickly and naturally develop a structured jet, which is

ahead of the slowly expanding cocoon. Further studies and detailed numerical simulations are needed to test this possibility.

- Abbott, B. P., et al. 2017a, *Physical Review Letters*, 119, 161101
- Abbott, B. P., et al. 2017b, *ApJL*, 848, L13
- Abbott, B. P., et al. 2017c, *ApJL*, 848, L12
- Abdo, A. A., Ackermann, M., Ajello, M., et al. 2009b, *ApJL*, 706, L138
- Abramowicz, M. A., Novikov, I. D., & Paczynski, B. 1991, *ApJ*, 369, 175
- Aloy, M. A., Janka, H.-T., & Müller, E. 2005, *A&A*, 436, 273
- Ardaneh, K., Cai, D., Nishikawa, K.-I., & Lembége, B. 2015, *ApJ*, 811, 57
- Bégué, D., & Pe'er, A. 2015, *ApJ*, 802, 134
- Bégué, D., Burgess, J. M., & Greiner, J. 2017, *ApJL*, 851, L19
- Beloborodov, A. M. 2011, *ApJ*, 737, 68
- Berger, E. 2014, *ARA&A*, 52, 43
- Bošnjak, Ž., Daigne, F., & Dubus, G. 2009, *A&A*, 498, 677
- Bromberg, O., Tchekhovskoy, A., Gottlieb, O., Nakar, E., & Piran, T. 2018, *MNRAS*, 475, 2971
- Burgess, J. M., Greiner, J., Bégué, D., & Berlato, F. 2017, *arXiv:1710.08362*
- Connaughton, V., Blackburn, L., Briggs, M. S., Broida, J., Burns, E. 2017, *LVC GRB Coordinates Network*, 21506
- Coulter, D. A., Foley, R. J., Kilpatrick, C. D., et al. 2017, *Science*, 358, 1556
- Dai, Z. G., & Gou, L. J. 2001, *ApJ*, 552, 72
- Daigne, F., Bošnjak, Ž., & Dubus, G. 2011, *A&A*, 526, A110
- Deng, W., & Zhang, B. 2014, *ApJ*, 785, 112
- Derishev, E. V. 2007, *Ap&SS*, 309, 157
- Eichler, D., Livio, M., Piran, T., & Schramm, D. N. 1989, *Nature*, 340, 126
- Fong, W., Berger, E., Margutti, R., & Zauderer, B. A. 2015, *ApJ*, 815, 102
- Gao, H., & Zhang, B. 2015, *ApJ*, 801, 103
- Geng, J.-J., Huang, Y.-F., Wu, X.-F., Zhang, B., & Zong, H.-S. 2018, *ApJS*, 234, 3
- Ghirlanda, G., Salafia, O. S., Pescalli, A., et al. 2016, *A&A*, 594, A84
- Giannios, D. 2006, *A&A*, 457, 763
- Goldstein, A., Veres, P., von Kienlin, A., Blackburn, L., Briggs, M. S. 2017a, *LVC GRB Coordinates Network*, 21528
- Goldstein, A., Veres, P., Burns, E., et al. 2017, *ApJL*, 848, L14
- Goodman, J. 1986, *ApJL*, 308, L47
- Gottlieb, O., Nakar, E., Piran, T., & Hotokezaka, K. 2017, *arXiv:1710.05896*
- Granot, J., Guetta, D., & Gill, R. 2017, *ApJL*, 850, L24
- Granot, J., Gill, R., Guetta, D., & De Colle, F. 2017b, *arXiv:1710.06421*
- Guo, F., Li, H., Daughton, W., & Liu, Y.-H. 2014, *Physical Review Letters*, 113, 155005
- Guo, F., Li, X., Li, H., et al. 2016, *ApJL*, 818, L9
- Hotokezaka, K., Kiuchi, K., Kyutoku, K., et al. 2013, *Phys. Rev. D*, 87, 024001
- Jin, Z.-P., Li, X., Wang, H., et al. 2017, *arXiv:1708.07008*
- Kasliwal, M. M., Nakar, E., Singer, L. P., et al. 2017, *Science*, 358, 1559
- Kathirgamaraju, A., Barniol Duran, R., & Giannios, D. 2018, *MNRAS*, 473, L121
- Komissarov, S. S., Vlahakis, N., & Königl, A. 2010, *MNRAS*, 407, 17
- Kumar, P., & Granot, J. 2003, *ApJ*, 591, 1075
- Lamb, G. P., & Kobayashi, S. 2017, *MNRAS*, 472, 4953
- Lazzati, D., Deich, A., Morsony, B. J., & Workman, J. C. 2017, *MNRAS*, 471, 1652
- Lazzati, D., Perna, R., Morsony, B. J., et al. 2017, *arXiv:1712.03237*
- Liang, E.-W., Yi, S.-X., Zhang, J., et al. 2010, *ApJ*, 725, 2209
- Longair, M. S. 2011, *High Energy Astrophysics* (3rd ed.; Cambridge: Cambridge Univ. Press)
- Lu, R.-J., Du, S.-S., Cheng, J.-G., et al. 2017, *arXiv:1710.06979*
- Lundman, C., Pe'er, A., & Ryde, F. 2013, *MNRAS*, 428, 2430
- Lü, J., Zou, Y.-C., Lei, W.-H., et al. 2012, *ApJ*, 751, 49
- Lyman, J. D., Lamb, G. P., Levan, A. J., et al. 2018, *arXiv:1801.02669*
- Mészáros, P., & Rees, M. J. 2000, *ApJ*, 530, 292
- Mészáros, P. 2002, *ARA&A*, 40, 137
- Mochkovitch, R., Hernanz, M., Isern, J., & Martin, X. 1993, *Nature*, 361, 236
- Moharana, R., & Piran, T. 2017, *MNRAS*, 472, L55
- Murguia-Berthier, A., Ramirez-Ruiz, E., Montes, G., et al. 2017, *ApJL*, 835, L34
- Nakar, E. 2007, *Phys. Rep.*, 442, 166
- Nakar, E., & Piran, T. 2017, *ApJ*, 834, 28
- Narayan, R., Paczynski, B., & Piran, T. 1992, *ApJL*, 395, L83
- Paczynski, B. 1986, *ApJL*, 308, L43
- Pe'er, A., Ryde, F., Wijers, R.A.M.J., Meszaros, P., & Rees, M. J. 2007, *ApJL*, 664, L1
- Pe'er, A. 2008, *ApJ*, 682, 463
- Pe'er, A., & Ryde, F. 2011, *ApJ*, 732, 49
- Pe'er, A., Barlow, H., O'Mahony, S., et al. 2015, *ApJ*, 813, 127
- Rees, M. J., & Mészáros, P. 1994, *ApJL*, 430, L93
- Rees, M. J., & Mészáros, P. 2005, *ApJ*, 628, 847
- Rossi, E., Lazzati, D., & Rees, M. J. 2002, *MNRAS*, 332, 945
- Rosswog, S., & Davies, M. B. 2002, *MNRAS*, 334, 481
- Rosswog, S., Ramirez-Ruiz, E., & Davies, M. B. 2003, *MNRAS*, 345, 1077
- Rosswog, S. 2013, *Philosophical Transactions of the Royal Society of London Series A*, 371, 20120272
- Rybicki, G. B. & Lightman, A. P. 1979, *Radiative processes in astrophysics*, New York, Wiley-Interscience
- Ryde, F. 2004, *ApJ*, 614, 827
- Ryde, F. 2005, *ApJL*, 625, L95
- Sapountzis, K., & Vlahakis, N. 2014, *Physics of Plasmas*, 21, 072124
- Sari, R., Piran, T., & Narayan, R. 1998, *ApJL*, 497, L17
- Savchenko, V., Mereghetti, S., Ferrigno, C., Kuulkers, E., & Bazzano, A. 2017, *LVC GRB Coordinates Network*, 21507
- Sironi, L., & Spitkovsky, A. 2014, *ApJL*, 783, L21
- Sun, H., Zhang, B., & Li, Z. 2015, *ApJ*, 812, 33
- Tchekhovskoy, A., McKinney, J. C., & Narayan, R. 2008, *MNRAS*, 388, 551
- Thompson, C. 1994, *MNRAS*, 270, 480
- Uhm, Z. L., & Zhang, B. 2014, *Nature Physics*, 10, 351
- Vurm, I., & Beloborodov, A. M. 2016, *ApJ*, 831, 175
- Xiao, D., Liu, L.-D., Dai, Z.-G., & Wu, X.-F. 2017, *ApJL*, 850, L41
- Xu, S., Yang, Y.-P., & Zhang, B. 2018, *ApJ*, 853, 43
- Xu, S., & Zhang, B. 2017, *ApJL*, 846, L28
- Zhang, B., & Mészáros, P. 2002a, *ApJ*, 571, 876
- Zhang, B., & Mészáros, P. 2002b, *ApJ*, 581, 1236
- Zhang, B., & Yan, H. 2011, *ApJ*, 726, 90
- Zhang, B.-B., Uhm, Z. L., Connaughton, V., Briggs, M. S., & Zhang, B. 2016a, *ApJ*, 816, 72
- Zhang, B.-B., Zhang, B., Castro-Tirado, A. J., et al. 2018a, *Nature Astronomy*, 2, 69
- Zhang, B.-B., Zhang, B., Sun, H., et al. 2018b, *Nature Communications*, 9, 447
- Zou, Y.-C., Wang, F.-F., Moharana, R., et al. 2018, *ApJL*, 852, L1